AGU PUBLICATIONS

JGR

Journal of Geophysical Research: Planets

RESEARCH ARTICLE

10.1002/2017JE005419

Equatorial Oscillation and Planetary Wave Activity in Saturn's Stratosphere Through the Cassini Epoch

S. Guerlet[1], T. Fouchet[2], A. Spiga[1,3], F. M. Flasar[4], L. N. Fletcher[5], B. E. Hesman[6], and N. Gorius[4]

[1]LMD/IPSL, Sorbonne Universités, UPMC Univ Paris 06, ENS, PSL Research University, École polytechnique, Université Paris Saclay, CNRS, Paris, France, [2]LESIA, Observatoire de Paris, PSL Research University, CNRS, Sorbonne Universités, UPMC Univ Paris 06, Univ. Paris Diderot, Sorbonne Paris Cité, Meudon, France, [3]Institut Universitaire de France, Paris, France, [4]NASA/GSFC, Greenbelt, MD, USA, [5]Department of Physics and Astronomy, University of Leicester, Leicester, UK, [6]StScI, Baltimore, MD, USA

Key Points:
- We characterize the vertical structure of Saturn's equatorial oscillation in 2015 from Cassini/CIRS limb data
- The descent rate of the oscillation and the vertical wind shear are larger in the upper stratosphere
- Planetary waves of zonal wave number 1 to 9 are frequently observed in the tropical stratosphere, including a Rossby wave identified in 2009

Supporting Information:
- Supporting Information S1
- Data Set S1
- Data Set S2
- Data Set S3
- Data Set S4
- Data Set S5
- Data Set S6

Correspondence to:
S. Guerlet,
sandrine.guerlet@lmd.jussieu.fr

Citation:
Guerlet, S., Fouchet, T., Spiga, A., Flasar, F. M., Fletcher, L. N., Hesman, B. E., & Gorius, N. (2018). Equatorial oscillation and planetary wave activity in Saturn's stratosphere through the Cassini epoch. *Journal of Geophysical Research: Planets, 123*, 246–261. https://doi.org/10.1002/2017JE005419

Received 10 AUG 2017
Accepted 2 JAN 2018
Accepted article online 9 JAN 2018
Published online 25 JAN 2018

©2018. American Geophysical Union. All Rights Reserved.

Abstract Thermal infrared spectra acquired by Cassini/Composite InfraRed Spectrometer (CIRS) in limb-viewing geometry in 2015 are used to derive 2-D latitude-pressure temperature and thermal wind maps. These maps are used to study the vertical structure and evolution of Saturn's equatorial oscillation (SEO), a dynamical phenomenon presenting similarities with the Earth's quasi-biennal oscillation (QBO) and semi-annual oscillation (SAO). We report that a new local wind maximum has appeared in 2015 in the upper stratosphere and derive the descent rates of other wind extrema through time. The phase of the oscillation observed in 2015, as compared to 2005 and 2010, remains consistent with a ~15 year period. The SEO does not propagate downward at a regular rate but exhibits faster descent rate in the upper stratosphere, combined with a greater vertical wind shear, compared to the lower stratosphere. Within the framework of a QBO-type oscillation, we estimate the absorbed wave momentum flux in the stratosphere to be on the order of $\sim 7 \times 10^{-6}$ N m^{-2}. On Earth, interactions between vertically propagating waves (both planetary and mesoscale) and the mean zonal flow drive the QBO and SAO. To broaden our knowledge on waves potentially driving Saturn's equatorial oscillation, we searched for thermal signatures of planetary waves in the tropical stratosphere using CIRS nadir spectra. Temperature anomalies of amplitude 1–4 K and zonal wave numbers 1 to 9 are frequently observed, and an equatorial Rossby ($n = 1$) wave of zonal wave number 3 is tentatively identified in November 2009.

Plain Language Summary Two aspects of tropical dynamics in Saturn's stratosphere are addressed: (1) the evolution, between 2005 and 2015, of an equatorial periodic oscillation in temperature and thermal wind and (2) the activity of planetary-scale waves. To do this, we analyze infrared spectra acquired by the Composite InfraRed Spectrometer instrument on board the Cassini spacecraft. These spectra are used to map Saturn's stratospheric temperature to identify the signature of waves and follow the evolution of the vertical structure of Saturn's equatorial oscillation. The latter is a dynamical phenomenon analogous to the Earth's quasi-biennal oscillation, semi-annual oscillation, and Jupiter's quasi-quadriennal oscillation and hence represents a unique case study of comparative planetology. These oscillations are thought to be driven by interactions between upward propagating waves and the mean zonal flow. We find that the phase of Saturn's oscillation in 2015 remains consistent with a period of 15 Earth years (half a Saturn year) and derive estimates of the momentum flux absorbed by waves. We report the observation of wave signatures with zonal wave numbers 1 to 9, among which an equatorial Rossby ($n = 1$) wave of zonal wave number 3. Altogether, these observations bring new constraints to future numerical models aiming at understanding Saturn's tropical dynamics.

1. Introduction

Like the Earth and Jupiter, Saturn's stratosphere harbors a periodic equatorial oscillation of its zonal wind and temperature vertical profiles, first discovered by Fouchet et al. (2008) and Orton et al. (2008). Given the similarities of their characteristics, the oscillations observed on these three planets are thought to be driven by similar dynamical processes and represent a unique case study of comparative planetology. On Earth, two main oscillations in zonal wind and temperature occur in the equatorial stratosphere: the quasi-biennal oscillation (QBO) in the lower stratosphere (15–30 km altitude or 100 hPa to 10 hPa) and the semi-annual

oscillation (SAO) that actually consists in two oscillations, with maximum amplitudes near the stratopause (45–50 km altitude, near 1 hPa) and near the mesopause (80 km altitude). Key processes in driving these oscillations involve interactions between upward propagating waves and the mean zonal flow (see Baldwin et al., 2001 for a review of the QBO and Garcia et al., 1997 for a climatology of the SAO). Waves with eastward and westward phase velocity are both invoked in this process, respectively, transporting eastward and westward momentum. When waves with eastward (westward) phase velocity are damped by breaking or being thermally dissipated, they preferentially deposit their momentum in an eastward (westward) shear zone below a jet maximum, leading to a descent of this shear zone. Altogether, these wave-zonal flow interactions lead to a vertical oscillation of the zonal wind profile and a descent of these wind extrema through the mesosphere and stratosphere. As a consequence, at a given pressure level, a (quasi)periodic oscillation of the zonally averaged zonal wind is observed over time. In addition to different vertical locations, the QBO and SAO differ by their periods: 6 months for the SAO and varying between 22 and 38 months for the QBO. These distinct periods reflect differences in their forcing mechanisms, which have a well-defined seasonal component for the SAO and not for the QBO. On gas giant planets, a single periodic equatorial oscillation has been identified in each of their middle atmospheres. The corresponding period has been estimated to 4 to 4.5 years for Jupiter's quasi-quadrennial oscillation (QQO) (Leovy et al., 1991) and 14.7 years for Saturn's equatorial oscillation (SEO) (Orton et al., 2008), about half a Saturn year. While the Earth's QBO seems to be a relevant analog of Jupiter's QQO, the semiannual period of the SEO raises the question whether Saturn's oscillation is more analogous to the Earth QBO or SAO, which will be discussed later.

The long period of the SEO makes its observational study a challenging task. Zonal wind speeds have never been directly measured in Saturn's stratosphere, so that the SEO is studied indirectly, by measuring temperature anomalies in thermal wind balance with the zonal flow. These anomalies are large, reaching $\pm$20 K on Saturn between the equator and 15° of latitude and reverse sign with altitude as the wind pattern oscillates (Fouchet et al., 2008; Guerlet et al., 2011). Due to these large temperature variations on relatively small vertical scales (two temperature and zonal wind extrema are separated by typically two pressure scale heights), these temperature anomalies have been best vertically resolved using Cassini radio occultation soundings (Schinder et al., 2011) and thermal infrared spectroscopic measurements in limb-viewing geometry by Cassini/Composite InfraRed Spectrometer (CIRS) (Guerlet et al., 2011). These two studies monitored the descent of the temperature anomalies between 2005/2006 and 2009/2010 with a poor temporal sampling but with a vertical resolution better than a scale height and a vertical coverage over three pressure decades (in the range 100 hPa to 0.1 hPa from radio occultations and 20 hPa to 0.01 hPa from CIRS limb data). In parallel, nadir observations by Cassini/CIRS (e.g., Fletcher et al., 2010) or from ground-based observations (broadband infrared spectroscopy; e.g., Orton et al., 2008) provide a great temporal coverage of the evolution of Saturn's temperatures in the middle stratosphere (5–0.5 hPa). Fletcher et al. (2017) exploited Cassini/CIRS nadir spectra recorded during 12 years. The authors report the regular downward propagation of SEO temperature anomalies between 2004 and 2011, followed by a sudden perturbation in 2011–2014 (attributed to the eruption of a tropospheric storm), then returning to its standard phase progression by 2015. One of the goals of our paper is to complement these results by deriving the structure of the oscillation in 2015 with greater vertical coverage and resolution.

Nadir observations by Cassini/CIRS can also provide unique longitudinal coverage of the temperature, which is highly valuable to study planetary waves potentially driving the SEO. On Earth, a broad spectrum of vertically propagating waves, from mesoscale gravity waves to planetary waves (both Kelvin and mixed Rossby-gravity waves), is thought to force the QBO and SAO (e.g., Dunkerton, 1991). On Saturn, several wave signatures have been reported in Saturn's upper troposphere at midlatitudes (Achterberg & Flasar, 1996; Orton & Yanamandra-Fisher, 2005) but our knowledge on stratospheric, equatorial waves is currently limited to the observation of temperature anomalies of wave number 9 in 2005/2006, identified as Rossby-gravity wave signatures (Liming et al., 2008). Further observations and characterization of the properties of equatorial waves in Saturn's stratosphere are needed to better understand its tropical dynamics and add constraints on the mechanism driving Saturn's equatorial oscillation.

In this paper, we extend Saturn's SEO monitoring by Cassini/CIRS limb measurements to 2015. From these infrared spectra, we retrieve the 2-D latitude-pressure cross section of the temperature and derive the associated thermal wind field between 30°N and 30°S, in the range 20 hPa–0.01 hPa. These maps are compared to previous analyses to discuss the evolution of the vertical structure of Saturn's SEO. We complete this study by analyzing Cassini/CIRS nadir data acquired between 2005 and 2015 to derive longitudinal temperature

Table 1
List of Cassini/CIRS Limb Data Sets Analyzed in This Study: Date, Latitude, and Projected Individual Field of View (FOV) on the Planet, Roughly Corresponding to the Vertical Resolution

Date	Latitude	Projected FOV
16/6/2015	25°S, 15°S, 2°N, 15°N	75 km
30/9/2015	10°S, 20°S, 30°S	53 km
24/11/2015	10°N, 20°N, 30°N	65 km

Note. For comparison, the pressure scale height is ~55 km in Saturn's stratosphere.

variations and monitor the thermal signature of planetary waves in Saturn's tropical stratosphere. The data analysis is presented in section 2. The results on the vertical structure of the SEO and wave activity are presented in sections 3 and 4, then these results are discussed and compared to the Earth case in section 5. We conclude in section 6.

2. Temperature Retrievals From Cassini/CIRS Observations

2.1. Analysis of Limb Observations

The Composite InfraRed Spectrometer (CIRS) on board the Cassini spacecraft has recorded spectra of Saturn's thermal infrared radiation in nadir or limb-viewing geometry between May 2004 and September 2017 at various spatial and spectral resolutions (Flasar et al., 2004). In this study we first exploit limb spectra acquired in June, September, and November 2015 probing latitudes between 30°N and 30°S at a spectral resolution of 15.5 cm^{-1} (see Table 1). These CIRS spectra are acquired by two of its three focal planes, FP3 and FP4, which cover respectively the ranges 590–1,100 cm^{-1} and 1,100–1,450 cm^{-1}. Each of these focal planes consists of an array of 10 detectors with an individual field of view of 0.273 × 0.273 mrad. This design is optimal for limb-viewing soundings, in which the arrays are set perpendicular to the limb of the planet. In this setting,

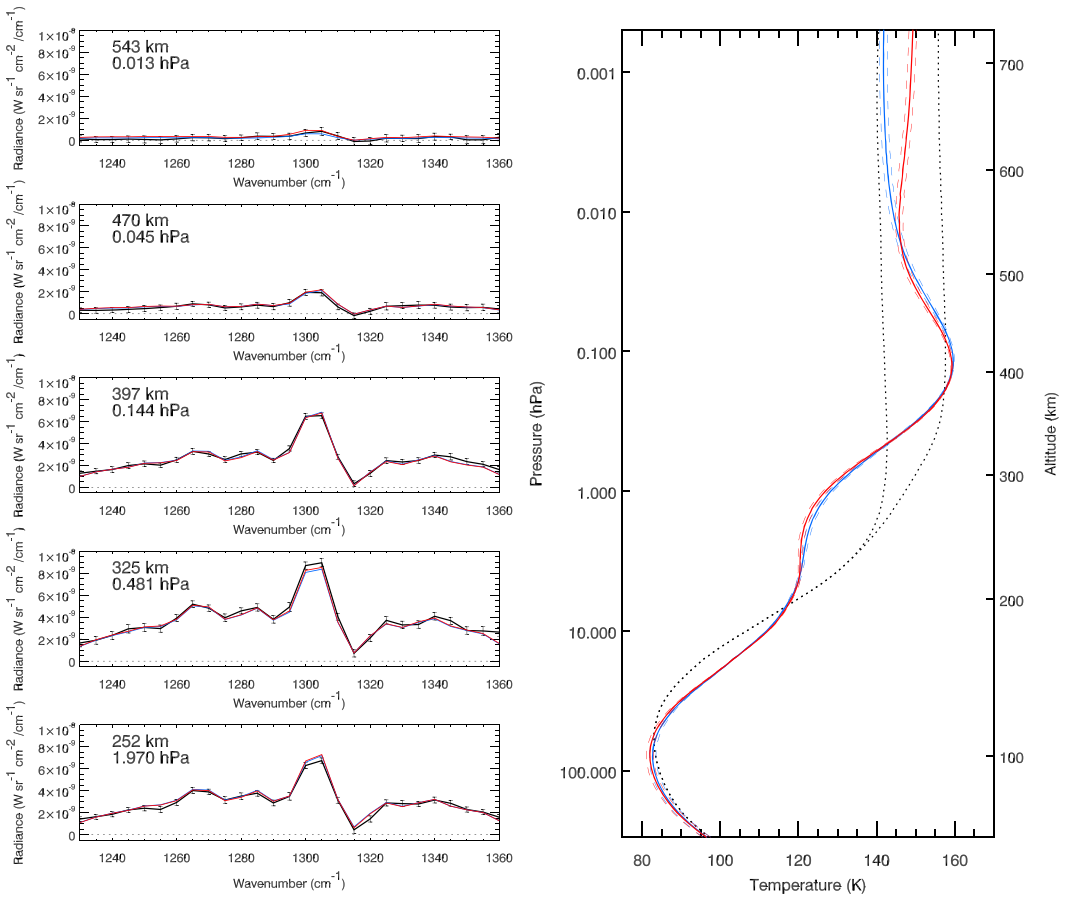


Figure 1. (left) Best fits (in red and blue, corresponding to different a priori profiles) to the ν_4 methane band observed by Cassini CIRS in limb-viewing geometry at 2°N (in black, with 1σ error bars). Spectra acquired at five different tangent altitudes are shown, which represent a subset of the eight spectra analyzed in total. Tangent altitudes and corresponding pressure levels are given in the upper left of each panel. (right) Corresponding retrieved profiles, in red and blue, starting from two different a priori profiles (black dotted lines). Above a certain level (here 0.01 hPa), the information content is poor and the temperature returns to the prior profile. In this example, we cannot discriminate between the two solutions (in blue and red) since the fits to the spectra are similar.

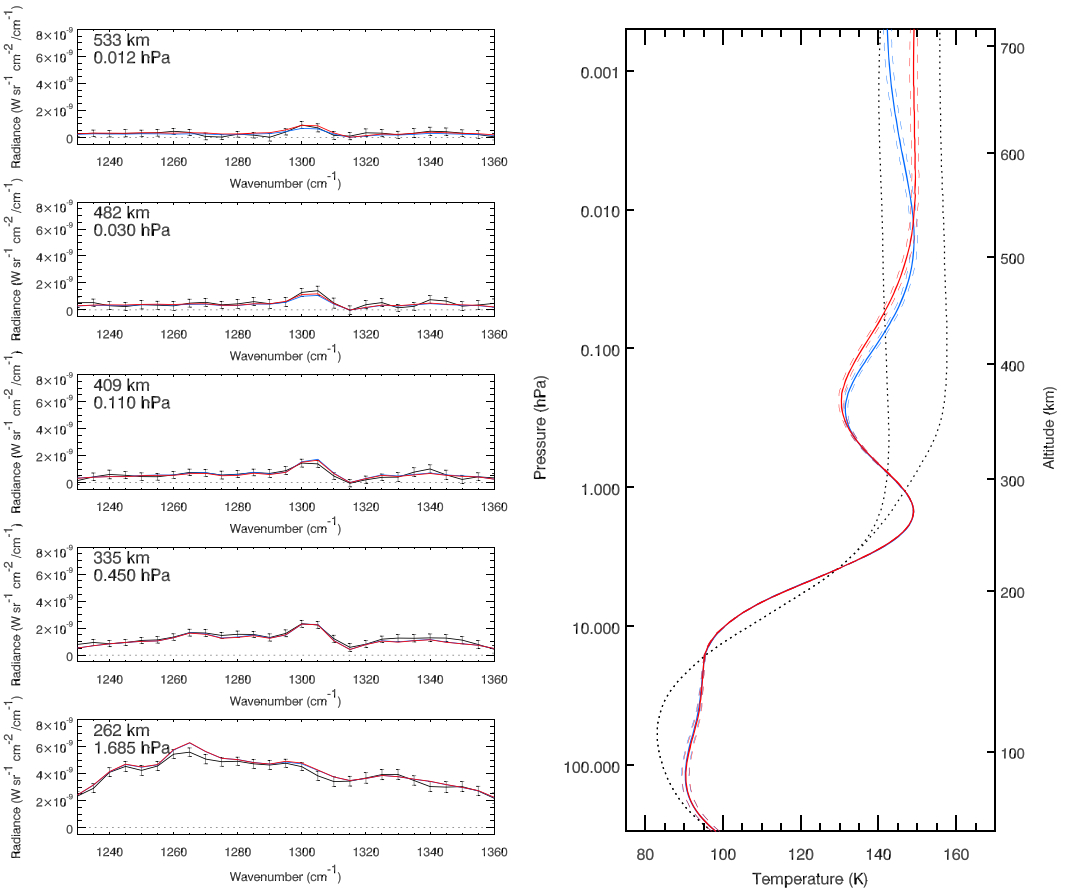


Figure 2. Same as Figure 1 but for latitude 15°S.

each detector probes a different tangent altitude with an individual field of view projected on the planet of 50–75 km, that is, about one atmospheric scale height in the vertical direction and less than 0.1° in latitude. For each latitude, all individual spectra acquired by a given FP3 or FP4 detector are then co-added to improve the signal-to-noise ratio, resulting in a set of 10 FP3 and 10 FP4 spectra, each corresponding to a different tangent height and altogether covering a vertical range of 10 atmospheric scale heights. These FP3 and FP4 spectra at different tangent heights are analyzed simultaneously to retrieve vertical profiles of the stratospheric temperature using a forward line-by-line radiative transfer model coupled to a retrieval algorithm. Information on the temperature is retrieved from (1) the 590–670 cm^{-1} region, dominated by the H_2 and He collision-induced continuum and probing the lower stratosphere (1–20 hPa) and (2) the 1,200–1,370 cm^{-1} region, dominated by the methane ν_4 emission band and probing the middle and upper stratosphere (0.005 hPa–5 hPa). Helium and dihydrogen are assumed to be homogeneously mixed in Saturn's stratosphere, and their mole fractions are set respectively to 0.1355 and 0.86, as derived by Conrath and Gautier (2000). The volume mixing ratio of methane is set to 4.5×10^{-3} in the troposphere (Flasar et al., 2004) and decreases in the upper stratosphere due to molecular diffusion and photochemistry, following Moses et al. (2000). Starting from an a priori temperature profile, an iterative process updates the temperature profile by minimizing a two-term cost function, one term representing the difference between synthetic and measured spectra and the other term being a regularization term, following the method of Conrath et al. (1998). The forward radiative transfer model and retrieval algorithm are further detailed in Guerlet et al. (2009) and Sylvestre et al. (2015).

Examples of fits to the ν_4 methane band and corresponding retrieved temperature profiles are shown in Figures 1 and 2 for latitudes 2°N and 15°S, respectively. Near the equator, a strong temperature increase with altitude is needed to reproduce the set of CIRS limb spectra, with temperatures of 120 K in the 1–5 hPa region reaching 160 K near the 0.1 hPa level. It corresponds to a strong emission of the *Q* branch of the ν_4 methane band (centered at 1,304 cm^{-1} and probing the middle and upper stratosphere) with respect to the *P* and *R* branches (centered at 1,270 and 1,340 cm^{-1} and probing lower levels). At 15°S, the shapes of the *P*, *Q*, and *R*

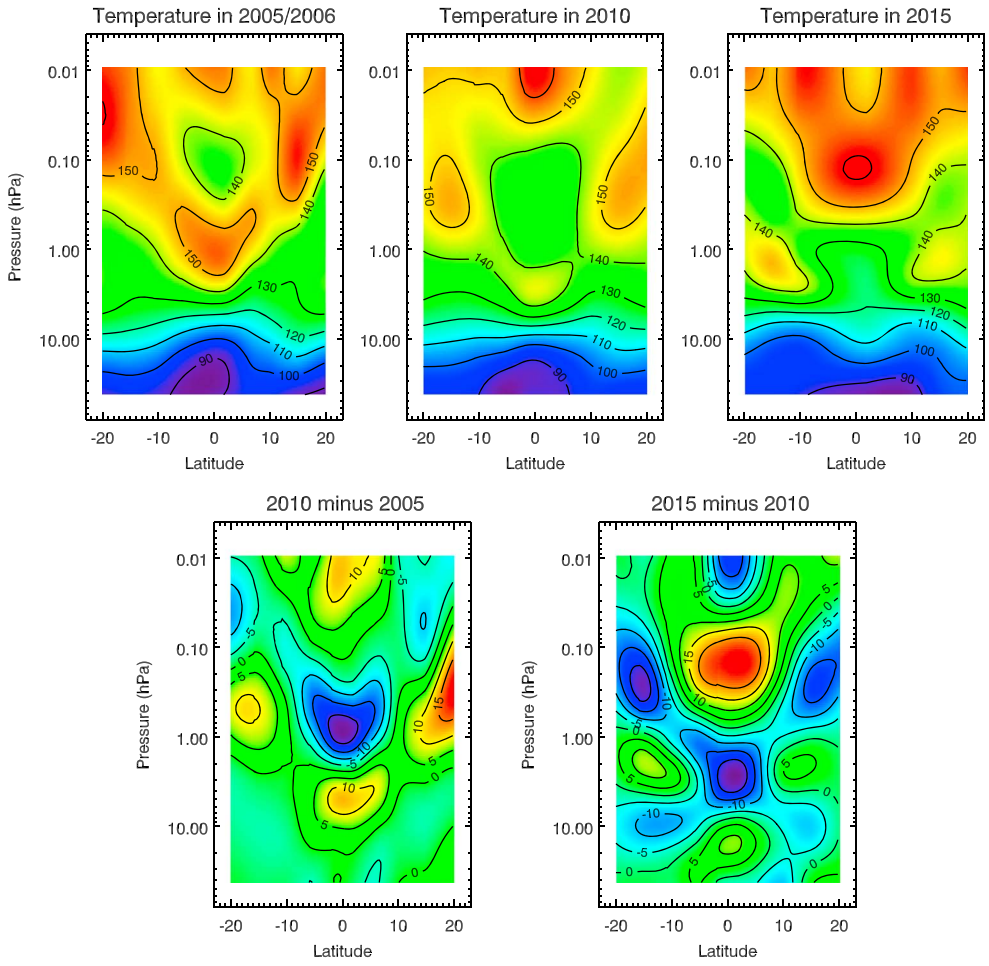


Figure 3. (top row) Latitude-pressure cross section of the temperature (in kelvin) obtained from Cassini/CIRS limb data acquired in 2005–2006 and February 2010 (top left and middle, slightly updated since Guerlet et al., 2011), June–November 2015 (top right, this work) and (bottom row) the difference in temperature between these dates.

branches are very different, with the *P* branch dominating the spectrum at a tangent pressure level of 1.7 hPa. These spectra can only be reproduced by a temperature profile featuring a local maximum in the lower stratosphere (probed by the *P* and *R* branches) and a local minimum at 0.2 hPa. Since this inverse problem is ill posed and underconstrained, the solution is not unique and partially depends on the a priori profile. Hence, to evaluate the robustness of our results, we systematically carry out several temperature retrievals, initialized with different a priori profiles. Retrieved profiles with the poorest fits of the data are discarded. Several retrieved profiles can correspond to similar fits to the data, as illustrated in Figures 1 and 2. These figures show that above the 0.01 hPa pressure level, the inverted temperature relaxes to the prior, as the information content of the spectra decreases. The retrieval error is of the order of 1 K (see also Guerlet et al., 2009 for a detailed error analysis), but the uncertainty linked to the choice of a priori profile can be greater (2–3 K in the range 0.1–0.01 hPa, e.g., at 15°S, as seen in Figure 2).

By combining these temperature profiles, we obtain the 2-D pressure-latitude temperature map shown in Figure 3 that will be discussed in section 3. For the sake of comparison, similar maps obtained from Cassini/CIRS limb data acquired in 2005/2006 and 2010 (Guerlet et al., 2011) are also shown along with the difference in temperature between the two epochs. We note that the co-addition of individual limb observations at a given latitude corresponds to sampling ~5° of the planet in longitude. When interpreting the results in section 3, we make the assumption that the temperature retrieved from the limb spectra is representative of the zonal mean temperature of the atmosphere. By doing so, we neglect the longitudinal temperature

Table 2
List of Cassini/CIRS Nadir Data Sets Analyzed in this Study: Date, Type (FIRMAP or MIRMAP), and Latitude

Date	Type	Latitude	Maximum peak-to-peak wave amplitude (K)	Dominant mode(s)
2/7/2005	MIRMAP	17°S	2 K	2; 7; 11
8/8/2005	MIRMAP	3°S	2 K	**6** ; 2
8/5/2006	MIRMAP	17°N	4 K	3; 6
4/11/2009	FIRMAP	20°N–3°N and 3°S–20°S		
		15°S	2.5 K	**3**; 1
		15°N	2.5 K	**3**; 1
5/12/2009	MIRMAP	2°N	1.5 K	4; 9
5/12/2009	MIRMAP	15°S	2.5 K	**3**
31/3/2010	MIRMAP	15°N	3 K	2; 4
7/4/2015	MIRMAP	17°S	4 K	**2**
13/5/2015	FIRMAP	5°N–20°N		
		15°N	2 K	1; 4
13/6/2015	FIRMAP	5°N–20°S		
		15°S	4.5 K	**1**; 2
		3°S	2 K	5; 2
2/9/2015	MIRMAP	15°S	3 K	**3**; **1**
2/9/2015	MIRMAP	3°S	2 K	**4**

Note. We also report the peak-to-peak amplitude of planetary wave signatures and their dominant modes, obtained from a periodogram analysis. Numbers in bold are for the modes that dominate the spectrum. Dates are formatted as day/month/year.

variations, which are small (2–3 K) compared to the meridional temperature variations (20–25 K). The longitudinal variations associated with potential wave activity are discussed in section 4.

2.2. Analysis of Nadir Observations

In order to search for thermal wave signatures, we employ the same retrieval algorithm to analyze CIRS nadir data of two types: "FIRMAP" observations, where the arrays of FP3 and FP4 scan an entire hemisphere at a time at the lowest spectral resolution (15.5 cm^{-1}) and "MIRMAP" observations, acquired at a resolution of 2.5 cm^{-1} but within a small latitudinal band. These two types of observations generally scan all 360° of the planet in longitude over a Saturn day and occasionally observe up to two successive rotations. In nadir viewing geometry, the H_2-H_2 and H_2-He continuum emission probes upper tropospheric temperatures (80–250 hPa) while the methane emission band probes mid-stratospheric temperatures (0.5–5 hPa). The typical vertical resolution is two scale heights for the 15.5 cm^{-1} resolution spectra, while the MIRMAP observations can better discriminate between the temperature at 5 and 0.5 hPa owing to their better spectral resolution.

In this paper we focus on nadir data acquired in the 20°N–20°S region in 2005/2006, 2009/2010, and 2015, that is, the three epochs for which we have already retrieved the full vertical temperature profile from limb observations (Fouchet et al., 2008; Guerlet et al., 2011; this paper). Table 2 summarizes the characteristics of those nadir data sets. Individual nadir spectra are co-added in 4°-wide latitude bins and 10°-wide longitude bins, with a step of 3° in latitude (only for the FIRMAP analyzes), 5° in longitude. Typically, 40 spectra are co-added in each bin at the resolution of 15.5 cm^{-1}, and 100 spectra are co-added at the resolution of 2.5 cm^{-1}. For each bin, the temperature retrievals are started from an a priori temperature profile corresponding to the closest (in latitude and time) limb retrieval available. This ensures a realistic vertical thermal structure for the retrieved profile in spite of the limited vertical information content of the nadir data. We obtain latitude-longitude temperature maps from three FIRMAPs acquired in November 2009, May 2015, and June 2015 and temperature longitudinal profiles at specific latitudes (equator, 15°N, 15°S) from nine MIRMAP sequences. Temperature anomalies at 1 hPa with respect to longitude are shown in Figure 4 for six examples: three near the equator and three near 15°S. A Lomb-Scargle periodogram analysis is performed in each case to evaluate the significance of these anomalies and extract their dominant modes, reported in Table 2. We note that, when starting from a generic a priori temperature profile instead of CIRS limb retrievals, very similar temperature anomalies as a function

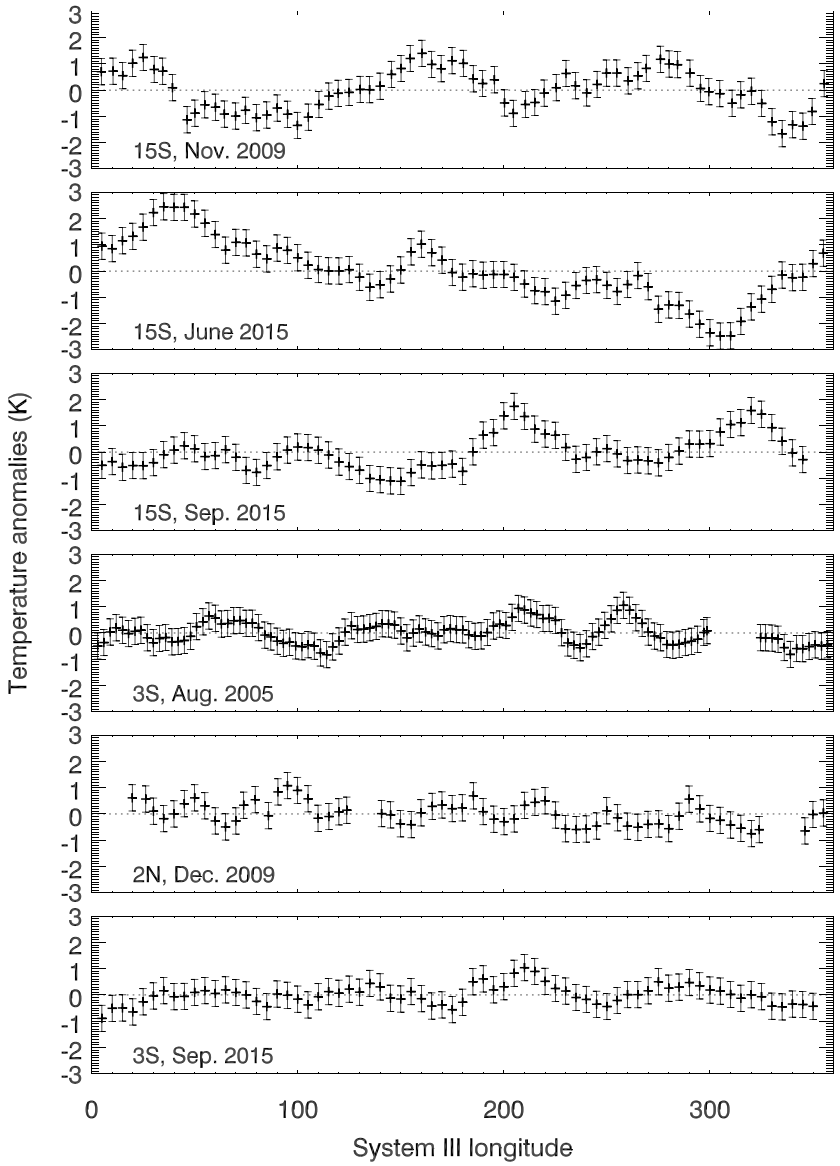


Figure 4. Temperature anomalies at 1 hPa (the zonal mean temperature has been subtracted in each case) retrieved from Cassini/CIRS nadir data as a function of longitude for different latitudes and dates, as labeled. A 1σ error bar is overplotted corresponding to the propagation of the noise level on the retrieved temperature. Other sources of uncertainty exist (e.g., the abundance of methane or the choice of a priori profile) but yield systematic errors, of about 1–2 K, not relevant for studying longitudinal temperature anomalies.

of longitude are obtained (but with different absolute values and vertical gradients); hence, the longitudinal wave signatures are independent of the choice of the prior profile. These wave signatures are discussed in section 4.

3. Results: The Evolution of the Equatorial Oscillation

3.1. Description of the Temperature and Thermal Wind Maps in 2015

Between 2010 and 2015, Saturn's tropical stratosphere has warmed and cooled in a complex way, as shown in Figure 3. The local temperature minima and maxima seen in 2010 have reversed to local maxima and minima in 2015. For instance, the equatorial stratosphere has warmed by 22 K (from 138 K to 160 K) at the 0.1 hPa level between 2010 and 2015, while it has cooled down by 21 K (from 143 K to 122 K) at the 2 hPa level. Furthermore, at a given pressure level, when the equator is warming (cooling), tropical latitudes at 15°S and 15°N experience cooling (warming). In contrast, from 2010 to 2015, our radiative-convective seasonal

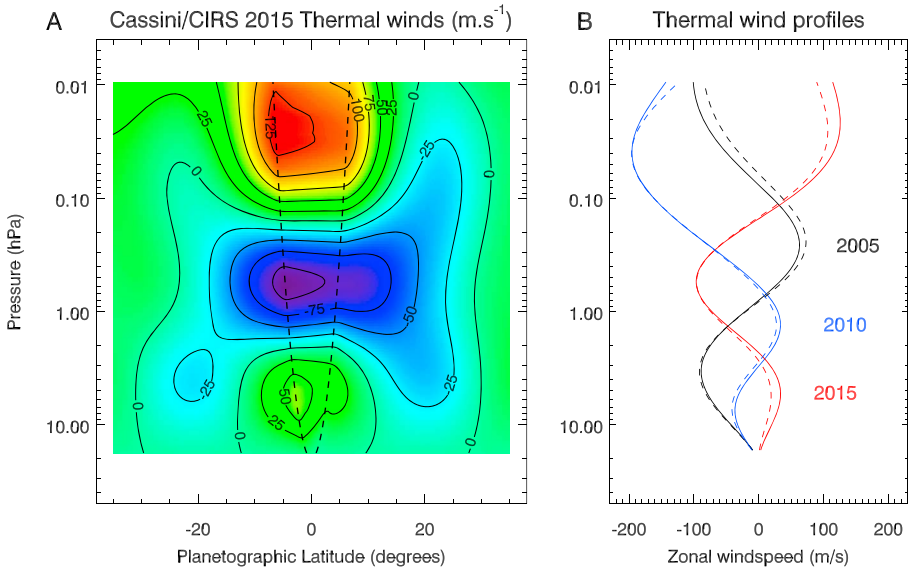


Figure 5. (a) Latitude-pressure cross section of the thermal zonal wind u in mid-2015 inferred from the temperature map shown in Figure 3, integrated from a boundary condition of $u = 0$ m s^{-1} at $p = 20$ hPa. The thermal wind equation cannot be applied within the dashed line, which defines the cylinder tangent to the equator at 20 hPa. Within this region, the wind field has been linearly interpolated on constant pressure surfaces. (b) Vertical profiles of the thermal wind at 7°S (solid lines) and 7°N (dashed lines) from 2005/2006 in black, February 2010 in blue, and mid-2015 in red. The error on u increases with altitude and is estimated to 4 m/s per scale height.

equilibrium model (Guerlet et al., 2014) predicts a negligible temperature change at the equator throughout the stratosphere, a moderate warming at 15°N (by 3 K to 6 K depending on the pressure level) as northern summer approaches and a significant cooling at 15°S (by 10 K to 15 K) as southern winter approaches, reinforced by ring shadowing. This model-observation mismatch strongly suggests that seasonal temperature changes in Saturn's tropical stratosphere are not solely governed by radiative processes. Rather, the observed extreme variations reflect a change in circulation associated with the descent of the wind extrema, in agreement with the interpretation built from previous observations (Guerlet et al., 2011; Fletcher et al., 2017; Schinder et al., 2011). Similarly, on Earth, a meridional residual circulation generates, through adiabatic vertical motions, the temperature gradients required to maintain thermal wind balance. As the oscillating wind pattern propagates downward, this residual circulation changes from locally rising (in westward shear zones) to locally sinking (in eastward shear zones) motions at the equator (Baldwin et al., 2001). While the 2005/2006 phase of Saturn's SEO corresponded to local equatorial subsidence at the 1 hPa pressure level, with a local temperature maximum and an observed equatorial enhancement of hydrocarbons (Fouchet et al., 2008; Guerlet et al., 2009), this situation reversed in 2015, as far as one can tell from the thermal structure.

We then integrate the modified thermal wind equation (Flasar et al., 2005; Fouchet et al., 2008) along cylinders concentric with the rotation axis to derive a map of the thermal zonal wind, shown in Figure 5a. Figure 5b compares near-equatorial (7°N and 7°S) vertical thermal wind profiles derived in 2005/2006, early 2010 and mid-2015. When integrating this equation, as the temperature is constrained only at and above the 20 hPa pressure level where absolute wind speeds are unknown, we arbitrary choose a boundary condition of zero wind at the 20 hPa pressure level. Hence, in the following, we discuss wind shear values and altitude of wind extrema at different epochs, but we do not interpret absolute wind speed temporal variations, since the (unknown) absolute wind speed at the 20 hPa level could vary with season while we kept a zero wind speed boundary condition through time. We also note that because the temperature meridional gradient is derived from observations acquired every ~5° in latitude, the resulting thermal wind field is also a smoothed representation of the true thermal wind field (small-scale variations are not captured).

As seen in Figure 5, the temperature meridional gradients in 2015 correspond to a local equatorial thermal wind minimum at 0.56 hPa of −100 m/s (relative to the 20 hPa level wind speed), surrounded by two local wind maxima, at 5.3 hPa and 0.02 hPa, of respective amplitude 40 m/s and 130 m/s. Hence, the vertical wind shear is the largest in the upper stratosphere (230 m/s over 2.9 scale heights H; hence, a shear of 79 m/s/H

Table 3
Wind Shear Between Two Local Wind Extrema at Different Epochs and Pressure Levels

Date	Mean pressure level	Δu	ΔH	Wind shear
2015	0.13 hPa	230 ± 24 m/s	2.9 *H*	79 ± 15 m/s/*H*
2010	0.26 hPa	257 ± 20 m/s	3.3 *H*	78 ± 12 m/s/*H*
2005	0.91 hPa	184 ± 15 m/s	2.6 *H*	71 ± 11 m/s/*H*
2015	1.7 hPa	140 ± 10 m/s	2.2 *H*	63 ± 9 m/s/*H*
2010	3.2 hPa	80 ± 5 m/s	1.7 *H*	47 ± 6 m/s/*H*

Note. H is the pressure scale height.

at an average pressure level of 0.13 hPa), while this shear is 140 m/s over 2.2 *H* (63 m/s/*H*) at an average pressure level of 1.7 hPa. Other values of the wind shear derived in 2005/2006 and early 2010 at different pressure levels are reported in Table 3. Altogether, these values depict an equatorial oscillation with a wind shear gradually increasing with altitude.

We caution that while we derive regions of positive and negative wind shear alternating with altitude, it is possible that the absolute wind remains eastward throughout the stratosphere. Indeed, using cloud-tracking measurements from Cassini and the Hubble Space Telescope, García-Melendo et al. (2010) and Sánchez-Lavega et al. (2016) report the existence of a broad prograde jet ±15° around the equator, with wind speeds of 370 ± 20 m/s in the deep troposphere ($p > 500$ hPa) decreasing to 300 ± 20m/s in the upper tropospheric haze level (60 hPa)—except in a narrow equatorial region where the zonal wind accelerates to 420 m/s. It is unknown how the zonal wind speed evolves between 60 hPa and 20 hPa (representing one pressure scale height), but our results suggest that a ~220 m/s zonal wind speed or greater at the 20 hPa level at subtropical latitudes would imply positive (eastward) wind speeds throughout the stratosphere.

3.2. Temporal Evolution of the Thermal Wind

Compared to the situation in 2005 and 2010, a new local eastward wind speed maximum has appeared in 2015 at low-pressure levels (0.03 hPa). By analogy with the mechanism proposed for the Earth's QBO, this new local maximum would originate from the deposition of eastward momentum by upward propagating waves at this pressure level (Baldwin et al., 2001). The source of this deposition is not known for Saturn, but radiative damping of the waves is one possibility. Holton and Lindzen (1972) proposed that mechanism for terrestrial QBO. From Figure 5, we can follow in 2015 the descent of two wind extrema that already existed in 2010, which complements previous results based on the 2005–2010 evolution (Guerlet et al., 2011). The previous local wind maximum (eastward) observed at 1.3 hPa in 2010 has descended to 5.3 hPa but is now weaker and much narrower in latitude, which is consistent with the idea that the SEO is damped in the lower stratosphere or at the tropopause level. If radiative damping is affecting the momentum exchange between the waves and background mean atmosphere, the weakening peak-to-peak amplitude of the wind maxima and minima may simply result from the radiative damping times becoming larger at higher pressures and lower temperatures found in the lower stratosphere. This would diminish the wave-mean atmosphere momentum exchange and slow the descent rate (see below). As the tropopause region is approached, eddy activity might also act to disrupt the descending pattern via mechanical dissipation.

Table 4 summarizes the descent rates of four wind extrema. These rates are not regular through the stratosphere: the wind extrema descend more rapidly in the upper stratosphere, with a rate of about 0.4 scale height per (Earth) year above the 0.5 hPa pressure level and slow down in the lower stratosphere, with a rate of typically 0.2–0.25 *H* per year below the 2 hPa pressure level. These rates are consistent with Schinder et al. (2011), who retrieved temperature vertical profiles in 2005 and 2010 from radio occultation soundings and derived a relatively slow descent rate of the temperature profile at the equator of 0.15 *H* per year at the ~5 hPa level. This may reflect the radiative damping times being longer at lower levels, resulting in less effective transfer of zonal momentum from the upwardly propagating waves to the mean zonal winds.

Table 4
Descent Rate of the Local Wind Extrema Between 2005 and 2010, and 2010 and 2015

Dates	Pressure levels of the wind extrema	Mean pressure level	Descent rate[a]
2/2010 to 8/2015 (66 months)	0.05 to 0.56 hPa	0.17 hPa	0.43 *H*/yr
1/2006 to 2/2010 (49 months)	0.25 to 1.33 hPa	0.58 hPa	0.40 *H*/yr
2/2010 to 8/2015	1.33 to 5.3 hPa	2.65 hPa	0.25 *H*/yr
1/2006 to 2/2010	3.35 to 7.5 hPa	4.9 hPa	0.19 *H*/yr

[a]Scale height per Earth year.

Projections can be made on when the thermal wind profile will resemble that observed in late 2005, so as to reevaluate the period of Saturn's SEO. Based on these descent rates, it would take almost 5 Earth years (58 months) for the new local wind maximum observed at 0.03 hPa in 2015 to descend to the 0.25 hPa pressure level (i.e., the location of the 2005 local maximum), for the measured rate of 0.43 *H*/yr. Similarly, for the local wind minimum seen at 0.56 hPa in 2015 to descend to 3.35 hPa would take 5.5 years, at rate of 0.33 *H*/yr (an intermediate rate relevant at these pressure levels — see Table 4). Hence, our calculations lead us to predict a similar SEO phase to that observed in late 2005 to occur in late 2020 or early 2021. This is consistent with the previously derived period of 14.7 ± 0.8 years by Orton et al. (2008). A recent study by Fletcher et al. (2017) based on Cassini/CIRS nadir data revealed how the Great Storm of 2010/2011 at Northern midlatitudes greatly disturbed Saturn's equatorial thermal structure. The authors find that these tropical temperature changes imply abrupt changes in the thermal wind profile, almost canceling the zonal wind vertical oscillation in the period 2011–2013, while in 2015 the SEO seemed to return to the phase it would have had if there had been no disruption by the storm. While CIRS limb sequences did not capture Saturn's SEO phase right after the storm, our study suggests that the observed phase of Saturn's SEO and associated descent rates in 2015 correspond, to first order, to the expected ones based on an ~15 year period. Hence, the perturbations induced by the 2010 Great Storm did not apparently modify Saturn's SEO period on long (seasonal) timescales, in agreement with the conclusion of Fletcher et al. (2017).

3.3. Descent Rates and Wave Forcing

In what follows, we make the working hypothesis that the mechanism driving the SEO is analogous to the one driving the Earth's QBO in order to relate the descent rates to the wave forcing. On Earth, the period of the QBO is controlled by the amount of vertical momentum flux carried by upward propagating waves: the transfer of momentum from the waves to the wind is responsible for driving the wind extrema downward at the observed rate. This downward propagation takes place within an overall tropical upwelling. The descent rates are also modulated by advection processes associated with the residual circulation: eastward shear zones indicate (through thermal wind balance) warm temperature anomalies at the equator maintained by local downwelling. Consequently, eastward shear zones are observed to descend faster than westward shear zones. On the contrary, the upward advection of momentum associated with westward shear inhibits their wave-induced descent (Baldwin et al., 2001).

Thus, the descent rates in Table 4 are the sum of two components: the wave-induced descent, which is not known a priori, and the descent and ascent in the shear zones due to the advective effect of the mean residual meridional circulation alone. Dunkerton (1991) shows that this rate $(dz/dt)_{advec}$, linked to the temperature anomalies, is proportional to the wind shear u_z

$$(dz/dt)_{advec} \sim -\alpha_T \beta L^2 u_z / N^2 \quad (1)$$

with N^2 the Brunt-Väisälä frequency, calculated to 5.5×10^{-5} s^{-2}; $\beta = 2\Omega/r$ at the equator, with r the planetary radius and Ω the angular rotation of Saturn; L the meridional scale of the equatorial confinement of the oscillation; and α_T the inverse of radiative timescale. Using an equilibrium radiative-convective model (Guerlet et al., 2014), the latter is evaluated to $\alpha_T \sim 10^{-8}$ s^{-1} at 1 hPa. Taking a width L of the order of 16° ± 2° (based on our thermal wind maps and the work of Fouchet et al., 2008) and a shear of 60 m/s/*H*, we find a rate of about 0.10 ± 0.02 *H*/yr at the 1 hPa pressure level. This value represents less than half the rate inferred from the thermal wind profiles (0.25 *H*/yr), suggesting that the descent or ascent due to the residual meridional circulation represents a moderate contribution to the overall descent in the lower stratosphere. However, at lower pressures, the radiative timescale becomes shorter (α_T increases by a factor of 3 at 0.1 hPa) and the inferred vertical wind shear is also larger (80 m/s/*H*): this implies rates of typically ~ 0.25–0.5 *H*/yr at the 0.1 hPa level. For a westward shear zone to exhibit a net descent rate of ~ 0.4 *H*/yr at 0.1 hPa (as observed in 2010–2015) in spite of an upward advection by the residual circulation of ~ 0.25–0.5 *H*/yr, then the actual descent rate forced by the wave momentum deposit must be even larger than the value reported in Table 4.

The vertical component of the wave momentum flux is conserved in the absence of wave-zonal flow interactions or decreases when waves deposit momentum in the atmosphere. An estimate of the vertical component of the wave momentum flux per unit density can be obtained by multiplying the wave-induced descent rate ($(dz/dt)_{wave}$) by the net zonal wind change between opposite phases of the oscillation (Dunkerton, 1991). These two factors are not precisely known, as the observed descent rates reported in Table 4 likely encompass the wave-induced descent and also upward/downward advection linked with the temperature anomalies

as explained above, and a potential overall tropical upwelling, as on Earth. There is indeed evidence for tropical upwelling in Saturn's upper troposphere (high equatorial clouds, high phosphine mixing ratio, and low para-H_2; Fletcher et al., 2010) that could penetrate the stratosphere. The net zonal wind change is also unknown, as we derive a thermal wind speed value relative to the 20 hPa wind speed, which could itself vary over time, and as wind speeds at the equator are interpolated. Nevertheless, we can provide order of magnitude estimates for this vertical momentum flux based on the near-equatorial thermal wind speeds and observed descent rates: at the 1 hPa level, a net wind change of ~140 m/s corresponds to a wave momentum flux per unit density of 0.06 $m^2\ s^{-2}$ or, multiplied by the density at 1 hPa, of 1.1×10^{-5} N m^{-2}; while at 0.1 hPa a wind change of ~200 m/s and a descent rate of 0.4–0.5 *H*/yr correspond to a momentum flux per unit density of the order of 0.15–0.18 $m^2 s^{-2}$ or 3–4 $\times 10^{-6}$ N m^{-2}. Hence, our observations are consistent with a wave momentum flux that decreases with altitude, with an absorbed wave flux of the order of $\sim 7 \times 10^{-6}$ N m^{-2} between 1 hPa and 0.1 hPa. These estimates provide rough constraints to future numerical models of Saturn's SEO.

Schinder et al. (2011) applied the same equation and multiplied the descent rate of 0.6 *H* in 4 Earth years (estimated at 5 mbar from their radio occultation measurements) by a net change in zonal wind of 200 m/s, which appears overestimated at the 5 mbar pressure level in the light of our study of temporal evolution of the thermal wind. Our study suggests that the net wind change is closer to 100 m/s at this pressure level, so that a revisited value for the estimated absorbed wave momentum flux per unit density is 0.025 $m^2 s^{-2}$ instead of 0.05 $m^2 s^{-2}$ (as published by Schinder et al., 2011). This corresponds to a flux of 2.5×10^{-5} N m^{-2} and is consistent with the fact that the vertical component of the wave momentum flux decreases with altitude.

We caution that the above estimates are obtained with the assumption that the descent rate of Saturn's equatorial oscillation is driven by momentum flux divergence carried by upward propagating equatorial waves. Other mechanisms involving seasonal wave activity, or the overturning of the meridional circulation, could also play a role in setting the period of the SEO to half a Saturn year, similarly to the Earth's SAO. We discuss these points in more detail in section 5.

4. Results: Equatorial Planetary Waves

Estimates of the vertical flux of momentum given in the previous section cannot be compared to observational constraints. This would require the measurement of anomalies in zonal and vertical winds which are inaccessible to Cassini observations. However, to broaden the knowledge on waves possibly driving the SEO, we can search for thermal signatures of planetary waves in the temperature fields retrieved from the Cassini/CIRS nadir spectra, as described in section 2.2. Examples of mid-stratospheric temperature anomalies at the 1 hPa level have been presented in Figure 4 and detailed in Table 2. In each period considered in our study (2005/2006, 2009/2010, and 2015), small temperature anomalies with respect to the zonal mean are frequently observed at the equator, of the order of 1.5 K, and larger temperature anomalies (1.5–4 K) are observed around 15°S and 15°N. From a Lomb-Scargle periodogram analysis, we find that about two thirds of the selected FIRMAP and MIRMAP observations at tropical latitudes correspond to statistically significant wave signatures, where one or two modes dominate the power spectrum. Hence, Saturn's tropical stratosphere seems prone to significant and regular wave activity. We report the observation of wave features of zonal wave numbers 1 to 4 at latitudes 15°N–20°N and 15°S–20°S. Higher wave numbers (4 to 9) are detected at the equator, although the smaller wave amplitudes make their identification less robust (see Table 2). Owing to the 10°-wide binning in longitude (5° step) of the CIRS nadir data, we cannot capture modes higher than wave number ~10.

The identification of the nature of equatorial wave modes (e.g., Kelvin, Rossby, and mixed Rossby-gravity) from these temperature disturbances is challenging and requires knowledge on wave parameters such as the westward or eastward phase speed and the meridional structure of the wave signature (e.g., symmetric or antisymmetric modes about the equator). The symmetry properties of the temperature anomalies are difficult to assess: unfortunately, the FIRMAP observing mode of Cassini generally scans a single hemisphere at a time, so that Saturn's southern and northern low latitudes are almost never observed simultaneously. There is one exception: in November 2009, a FIRMAP covering the Northern Hemisphere extended to 20°S. The corresponding temperature map, shown in Figure 6 (top) at 0.5 hPa, exhibits wave patterns of zonal wave number 3 at 15°N and 15°S, with peak-to-peak temperature anomalies of 2.5 K symmetric about the equator. Longitudinal cross sections of the temperature anomalies at 15°N and 15°S, with the corresponding

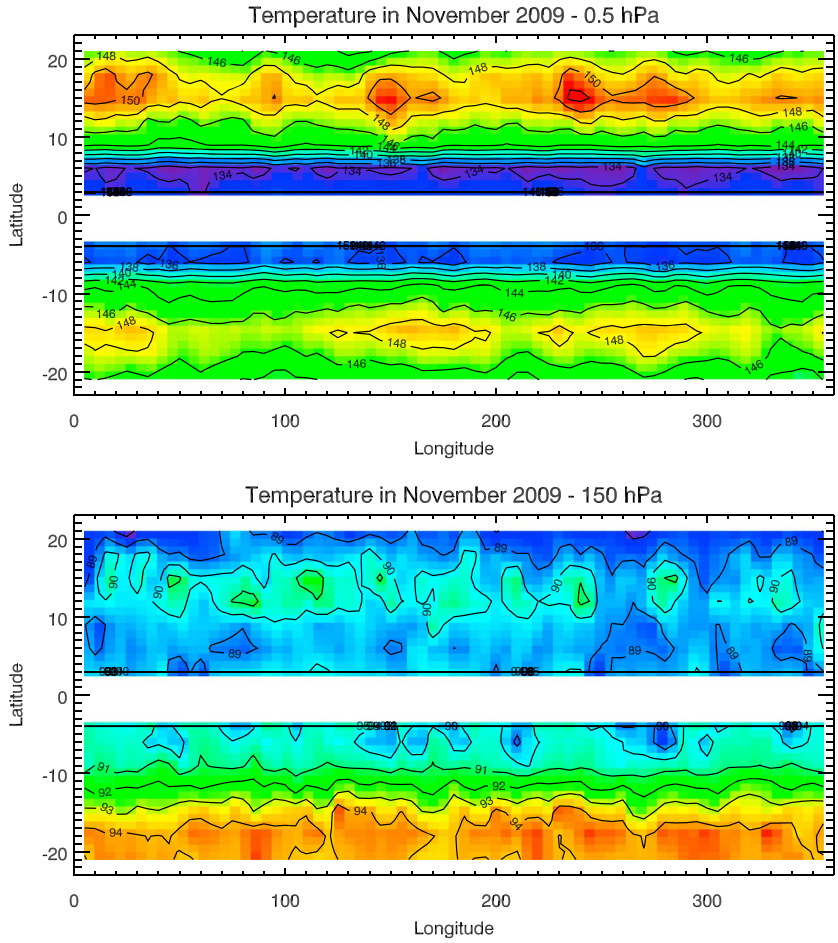


Figure 6. Maps of the temperature at (top) 0.5 hPa and (bottom) 150 hPa (retrieved from a Cassini/CIRS FIRMAP in November 2009. At 0.5 hPa, thermal waves with a peak-to-peak amplitude of 2.5 K and wave number 3 are clearly visible at both 15°S and 15°N. Spectra were co-added in bins of 10° wide in longitude, with a step of 5°, and bins 4° wide in latitude, with a step of 3°. The equatorial region is missing as the rings were contaminating the spectra in this region.

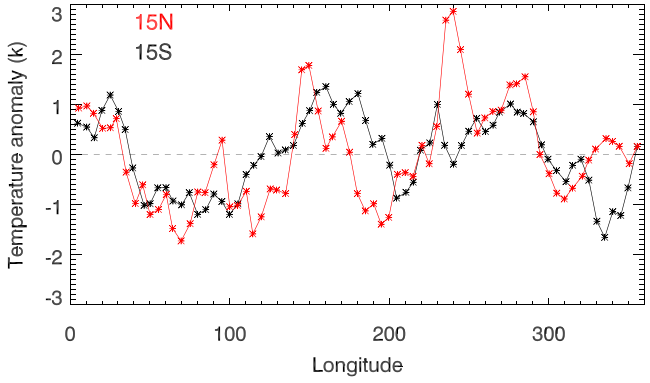


Figure 7. Temperature anomalies at 0.5 hPa as a function of longitude overplotted at 15°N, in red, and 15°S, in black (the zonal mean temperature for each latitude has been removed) obtained from the FIRMAP in November 2009.

Lomb-Scargle periodograms, are shown in Figures 7 and 8, respectively. Equatorial waves theory—in the framework of beta-plane approximation (Matsuno, 1966)—indicates that this configuration (subtropical temperature extrema symmetric about the equator) is a characteristic of an equatorial Rossby wave with $n = 1$ and $s = 3$. Here the solutions for equatorial wave modes are labeled by two numbers, s and n, where s is the zonal wave number and n is the order of the Hermite function describing the mode's meridional structure. Boyd (1978) further showed that the Rossby ($n = 1$) wave mode retains its symmetric signature even in the presence of a meridional wind shear (as is the case on Saturn).

We notice a more complex stratospheric wave activity at 15°N than at 15°S in the 2009 map. An examination of the temperature retrieved in the upper troposphere (150 hPa, shown in Figure 6, bottom) reveals that, at this epoch, the northern tropical latitudes were close to barotropic conditions (small meridional temperature gradient), while the baroclinicity is larger in the southern tropics. Some high-wave number wave activity is suspected in the upper troposphere at 15°N and coincides with a more complex stratospheric wave activity at 15°N. The near-barotropic conditions at 15°N imply a weak vertical shear of the zonal wind, while the meridional

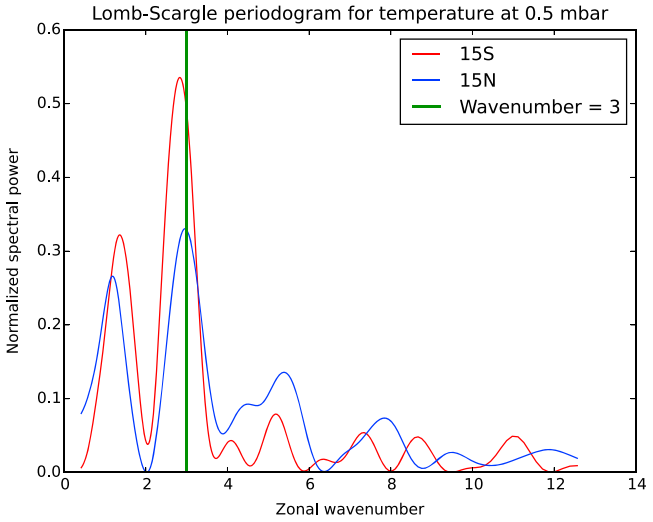


Figure 8. Lomb-scargle periodograms at 0.5 hPa for 15°N and 15°S from the FIRMAP in November 2009. A wave number 3 feature dominates the two power spectra.

temperature gradient at 15°S implies that the zonal jet decreases with altitude. This trend is in agreement with the results of Fletcher et al. (2016), who provide a 10 year record of tropospheric temperature and thermal wind fields based on Cassini/CIRS nadir data. For the year 2009, they derive a thermal wind decreasing from 300 m/s at the 500 hPa to 240 m/s at 100 hPa at 15°S and a near-constant thermal wind (300 m/s) at 15°N. Hence, a greater variety of vertically propagating waves could be transmitted to the stratosphere at 15°N compared to 15°S, which might explain the different observed wave activities in Figure 6. Finally, although we favor the interpretation of the signature of a Rossby ($n = 1$) equatorial wave, we cannot exclude that the two stratospheric wave signatures observed at 15°S and 15°N are two distinct waves originating from jet instabilities (barotropic or baroclinic) that would coincidently have the same zonal wave number 3 and be in phase.

Rossby waves are characterized by a westward phase speed. Determining the phase speed of waves requires observations ideally separated by one or a few Saturn days (performed only in rare occasions) as well as knowledge of the background zonal wind speed to infer the eastward or westward propagation with respect to the mean zonal flow. In December 2009, a MIRMAP observation covered latitude 15°S during 1.3 Saturn rotation, meaning that a third of the planet (in longitude) was mapped twice ~11 h apart. We report the observation of temperature anomalies of amplitude 2.5 K at the 0.5 hPa level (see Figure 9), consistent with a wave number 3 mode that could be reminiscent of the wave we observed in November 2009. The two successive rotations reveal a wave pattern stationary with respect to System III longitudes (absolute phase speed $c = 0$ m s^{-1}). At this latitude, the background flow u has been previously estimated to be +250 m/s eastward at the 1 hPa level (from cloud-tracking measurements at 500 hPa combined with tropospheric and stratospheric thermal wind speeds derived by Liming et al., 2008). A wave with an intrinsic phase speed of 0 m s^{-1} would travel 9° eastward in 11 h with respect to the observer (due to the 250 m/s background wind), which is not observed but would have been detectable (see Figure 9). Thus, we can infer that this wave has a westward propagation with respect to the background wind, with an intrinsic phase speed $c - u$ estimated to be -250 ± 80 m/s. The ± 80 m/s error estimates correspond to a $\pm 3°$ longitudinal shift within which the two temperature data sets (from the two Saturn rotations) agree, within error bars. This observation supports the identification of the same Rossby wave for both the November and December 2009 data, as this wave mode is characterized by a westward propagation. We note that the amplitude of the wave signature is greater at 1–0.5 hPa than at 5 hPa, consistent with the amplification of Rossby wave signatures as density decreases.

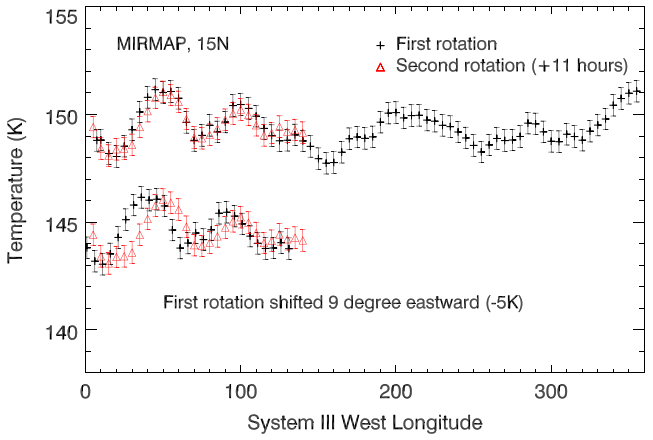


Figure 9. Temperature at 0.5 hPa retrieved at 15°S from the MIRMAP in December 2009 as a function of longitude, and covering 1.3 Saturn rotation. The first rotation is displayed as black crosses, while the second partial rotation is shown as red triangles. Spectra were co-added in bins of 10° wide in longitude, with a step of 5°. The wave signature appears stationary in System III and therefore must propagate westward with respect to the background flow, estimated to 250 m/s. Lower curve: to simulate the propagation due to the background zonal wind between the two rotations, these temperatures are reproduced with a −5 K offset and a 9° eastward displacement of the first rotation.

Finally, we investigate if a Rossby wave can propagate vertically in such a strong eastward background flow, where this Rossby wave could become evanescent. From the Rossby wave dispersion relation, one can define a critical velocity u_c for which the vertical propagation of Rossby waves is possible, expressed as follows (Andrews et al., 1987):

$$u_c = \frac{\beta}{k^2 + l^2 + \frac{f^2}{4N^2H^2}} \quad (2)$$

with $k = \frac{2\pi}{\lambda_x}$, $l = \frac{2\pi}{\lambda_y}$ (where λ_x and λ_y are the zonal and meridional wavelengths), and f the Coriolis parameter ($f = 2\Omega\sin\theta$ at latitude θ). At a latitude of 15°, taking $f = 8.4 \times 10^{-5}$ s^{-1} and a scale height of 50 km yields $u_c = 310$ m/s for a wave number 3 Rossby wave. The vertical propagation is possible if $u - c < u_c$. Considering an absolute phase speed $c = 0$ m s^{-1}—consistent with the wave observed at 15°S—and the wind measurements (and thermal wind calculations) of 250–300 m/s reported

at 15° latitude by García-Melendo et al. (2010) and Liming et al. (2008) in the lower and middle stratosphere, the vertical propagation of the Rossby wave observed at 15°S is thus allowed.

5. Discussion

In this paper, we have further characterized the vertical structure of the SEO, its descent rates, and vertical wind shears at different pressure levels. Furthermore, we have extended the observations of equatorial planetary waves compared to previous analyses. The only previous characterization of stratospheric, equatorial waves is reported by Liming et al. (2008), from Cassini/CIRS nadir data acquired in 2005–2006. The authors that derived temperature anomalies of small amplitude (0.5–1 K), of zonal wave number 9 (similar to the one we report at 2°N in December 2009—see Table 2), inferred a westward propagation for those waves and tentatively identified them as mixed Rossby-gravity modes. We caution, however, that this wave mode is characterized by an antisymmetric temperature signature across the equator, at odds with the temperature maps derived by Liming et al. (2008) that exhibit temperature anomalies maximum at the equator (compatible with westward inertia-gravity wave signatures). A global survey of tropospheric and stratospheric planetary wave activity, both tropical and extratropical, has been initiated by Orton et al. (2013) using ground-based and Cassini observations since 2003. The authors report frequent observations of planetary waves at latitudes 30°–45°S and 0°–30°N; however, the nature of these waves remains to be assessed. The ($n = 1$) Rossby equatorial wave mode that we tentatively identify in Cassini/CIRS 2009 observations is thus the first of its kind observed in Saturn's stratosphere. We note that this Rossby mode was identified by several studies in Jupiter's upper troposphere (Allison, 1990; Flasar & Conrath, 1994; Ortiz et al., 1998). In particular, from Voyager/IRIS data, Flasar and Conrath (1994) identified a wave number 1 temperature anomaly in Jupiter's atmosphere that was in phase between 28°N and 20°S despite the significant variations of the zonal wind, similar to the wave signature reported in our study.

On Earth, a broad spectrum of waves, from inertia-gravity to planetary waves, contributes to driving the QBO and SAO, although it has been shown that the ($n = 1$) Rossby wave has a minor contribution to the forcing of the QBO (Takahashi & Holton, 1991). On Jupiter, several models were able to broadly reproduce the descending pattern of the quasi-quadrennial oscillation (QQO), either with planetary wave forcing alone (Li & Read, 2000) or achieving more satisfactory results with small-scale gravity waves (Friedson, 1999). Yet neither of these studies completely reproduce the observed temperature anomalies. Hence, the contribution of different wave types to the forcing of Saturn's SEO or Jupiter's QQO is still an open question. Another open question is the role of seasonal forcing in setting the quasi semiannual period of Saturn's SEO. Indeed, on Earth, the SAO is thought to be locked to the seasonal cycle through seasonal Rossby wave activity (more intense in the summer hemisphere) and/or the meridional circulation, carrying westward momentum through the equator twice a year. Whether the same argument applies to Saturn is still unknown.

We summarize below the similarities and differences between Saturn's equatorial oscillation and the Earth's QBO and SAO.

1. The downward propagation of Saturn's oscillation extends almost to the tropopause (Schinder et al., 2011). The eastward and westward shear zones descend rather regularly, at least in the range 5–0.5 hPa (see, e.g., Figure 3 in Fletcher et al., 2017). This is strikingly analogous to the QBO pattern, but not to the SAO pattern, for which the downward propagation is limited mainly to the eastward phase (Andrews et al., 1987).
2. The SAO has a maximum amplitude at the stratopause and mesopause levels, with a minimum amplitude in between (Garcia et al., 1997). Our work shows no such region of minimum in the thermal wind amplitude in Saturn's middle atmosphere.
3. The period of half a Saturn year for the SEO advocates for a seasonal forcing and a mechanism similar to the Earth's SAO. There is indeed evidence that the transmittivity of waves may vary with seasons in the troposphere (Fletcher et al., 2016), but the impact on the wave-zonal flow interactions needs to be quantitatively assessed. Similarly, a seasonally dependent meridional stratospheric circulation—favorable for the SAO analog—is speculated from the observation of anomalies in the temperature and hydrocarbon fields (Guerlet et al., 2009; Sinclair et al., 2014) but its amplitude is still poorly known.

Hence, Saturn's equatorial oscillation exhibits unique morphology and characteristics, with (somewhat conflicting) similarities with both the QBO and SAO.

6. Conclusion

We have analyzed thermal infrared observations by Cassini/CIRS to monitor the evolution of the vertical structure of Saturn's stratospheric equatorial oscillation in 2015 and to search for associated tropical planetary wave activity in 2006, 2009/2010, and 2015. We report that a new local wind maximum has appeared in 2015 at low-pressure levels (0.03 hPa), while the previous local wind maximum derived in 2010 in the lower stratosphere is slowly vanishing. We estimate the descent rates of wind extrema at different pressure levels, ranging from typically 0.2 scale height H per (Earth) year at 5 hPa to 0.4 H/yr at 0.1 hPa. Hence, the SEO does not propagate downward as a solid body but exhibits faster descent rate in the upper stratosphere combined with a greater wind shear. Furthermore, in the framework of a QBO-like mechanism where the amount of vertical wave momentum flux controls the period of the oscillation, we estimated the vertical component of the wave momentum flux necessary to explain our observations. The corresponding order of magnitude of the absorbed wave flux between 1 hPa and 0.1 hPa is estimated to be $\sim 7 \times 10^{-6}$ N m^{-2}.

On Earth, tropical convection generates a broad spectrum of waves, from mesoscale gravity waves, synoptic-scale inertia-gravity waves to planetary-scale Rossby, mixed Rossby-gravity and Kelvin waves, all of which contribute to driving the QBO. The vertical flux of momentum due to planetary waves alone is thought to contribute to roughly one third of the required flux needed to drive the QBO (Baldwin et al., 2001). On Saturn, Liming et al. (2008) already reported the detection of a wave number 9 mixed Rossby-gravity wave or westward inertia-gravity wave, while we tentatively report for the first time the observation of a wave number 3 Rossby ($n = 1$) equatorial mode in November 2009 and more generally significant wave activity at subtropical latitudes (15°N, 15°S). Planetary waves with low wave numbers (1–4) are almost systematically found at subtropical latitudes, while higher (4–9) wave numbers are observed at the equator; however, the reason for this difference is not known yet.

The seasonal variability of planetary waves is thought to play a role in setting the 6 month period of the terrestrial SAO. The phase of the QBO itself modulates stratospheric wave transmittivity and activity (Yang et al., 2012), both at tropical and extratropical latitudes, and impacts in turn the phase of the mesospheric SAO (Garcia et al., 1997). Hence, there is a complex interplay between the wave activity, the atmospheric wave transmittivity, and the zonal wind profile. On Saturn, such a variability in planetary wave activity could be further studied, for instance, through a complete survey of planetary waves spanning the entire Cassini mission (beyond the scope of this paper, but initiated by Orton et al., 2013). In addition, radio occultation measurements by Cassini/RSS could be further exploited to detect and characterize mesoscale gravity waves. In the future, monitoring the evolution of Saturn's equatorial oscillation beyond the Cassini era will have to rely on ground-based spectroscopic measurements or with instruments on board the James Webb Space Telescope.

Modeling efforts are still needed to reproduce the SEO and understand the role of different equatorial, nonequatorial waves, and the meridional circulation in driving and maintaining this dynamical oscillation. Several general circulation models have been developed for gas giants' stratospheres (Friedson & Moses, 2012; Spiga et al., 2016). These models will have to account for the observed period, descent rate, amplitude, and vertical extent of the SEO as reported in this paper and others (Fletcher et al., 2017; Schinder et al., 2011). Modeling the SEO represents a numerical challenge, as do the QBO and SAO on Earth, as it requires (i) a high vertical resolution to properly represent the wave-mean flow interaction in the wind shear zones, (ii) a parameterization of unresolved small-scale gravity waves, and (iii) a good representation of the meridional circulation, which is still poorly achieved for Saturn's stratosphere. The question whether Saturn's SEO is more analogous to either the Earth's QBO or SAO, or has a combination of seasonal and nonseasonal forcing of its own, is still an open question.

Acknowledgments
Guerlet, Fouchet, and Spiga are supported by the Centre National d'Etudes Spatiales (CNES). Fletcher was supported by the Royal Society research fellowship and European Research Council consolidator grant at the University of Leicester. This work is based on data analysis acquired by the CIRS instrument on board the Cassini spacecraft. We thank François Lott for interesting discussions on the Earth's QBO. We are grateful to the Cassini/CIRS team for their hard work in planning and calibrating the spectra. The results presented in this paper (temperature profiles retrieved from Cassini/CIRS limb and nadir data) are available as supporting information and/or can be obtained by contacting the first author. We thank two anonymous reviewers for their constructive reviews of this manuscript.

References

Achterberg, R. K., & Flasar, F. M. (1996). Planetary-scale thermal waves in Saturn's upper troposphere. *Icarus*, *119*, 350–369. https://doi.org/10.1006/icar.1996.0024

Allison, M. (1990). Planetary waves in Jupiter's equatorial atmosphere. *Icarus*, *83*, 282–307. https://doi.org/10.1016/0019-1035(90)90069-L

Andrews, D., Holton, J., & Leovy, C. (1987). *Middle atmosphere dynamics*. New York: Academic Press.

Baldwin, M. P., Gray, L. J., Dunkerton, T. J., Hamilton, K., Haynes, P. H., Randel, W. J., … Takahashi, M. (2001). The quasi-biennial oscillation. *Reviews of Geophysics*, *39*, 179–229. https://doi.org/10.1029/1999RG000073

Boyd, J. P. (1978). The effects of latitudinal shear on equatorial waves. Part II: Applications to the atmosphere. *Journal of Atmospheric Sciences*, *35*, 2259–2267. https://doi.org/10.1175/1520-0469(1978)035 2259: TEOLSO 2.0.CO;2

Conrath, B. J., & Gautier, D. (2000). Saturn helium abundance: A reanalysis of voyager measurements. *Icarus*, *144*, 124–134. https://doi.org/10.1006/icar.1999.6265

Conrath, B. J., Gierasch, P. J., & Ustinov, E. A. (1998). Thermal structure and para hydrogen fraction on the outer planets from voyager IRIS measurements. *Icarus*, *135*, 501–517. https://doi.org/10.1006/icar.1998.6000

Dunkerton, T. J. (1991). Nonlinear propagation of zonal winds in an atmosphere with Newtonian cooling and equatorial wavedriving. *Journal of Atmospheric Sciences*, *48*, 236–263.

Flasar, F. M., & Conrath, B. J. (1994). Thermal waves in Jupiter's atmosphere. In *AAS/Division for Planetary Sciences Meeting Abstracts #26, Bulletin of the American Astronomical Society* (Vol. 26, p. 1103).

Flasar, F. M., Kunde, V. G., Abbas, M. M., Achterberg, R. K., Ade, P., Barucci, A., … Taylor, F. W. (2004). Exploring the Saturn system in the thermal infrared: The composite infrared spectrometer. *Space Science Reviews*, *115*, 169–297. https://doi.org/10.1007/s11214-004-1454-9

Flasar, F. M., Achterberg, R. K., Conrath, B. J., Gierasch, P. J., Kunde, V. G., Nixon, C. A., … Wishnow, E. H. (2005). Titan's atmospheric temperatures, winds, and composition. *Science*, *308*, 975–978. https://doi.org/10.1126/science.1111150

Fletcher, L. N., Achterberg, R. K., Greathouse, T. K., Orton, G. S., Conrath, B. J., Simon-Miller, A. A., … Flasar, F. M. (2010). Seasonal change on Saturn from Cassini/CIRS observations, 2004–2009. *Icarus*, *208*, 337–352. https://doi.org/10.1016/j.icarus.2010.01.022

Fletcher, L. N., Guerlet, S., Orton, G. S., Cosentino, R. G., Fouchet, T., Irwin, P. G. J., … Morales-Juberías, R. (2017). Disruption of saturn's quasi-periodic equatorial oscillation by the great northern storm. *Nature Astronomy*, *1*, 765–770. https://doi.org/10.1038/s41550-017-0271-5

Fletcher, L. N., Irwin, P. G. J., Achterberg, R. K., Orton, G. S., & Flasar, F. M. (2016). Seasonal variability of Saturn's tropospheric temperatures, winds and para-H_2 from Cassini far-IR spectroscopy. *Icarus*, *264*, 137–159. https://doi.org/10.1016/j.icarus.2015.09.009

Fouchet, T., Guerlet, S., Strobel, D. F., Simon-Miller, A. A., Bézard, B., & Flasar, F. M. (2008). An equatorial oscillation in Saturn's middle atmosphere. *Nature*, *453*, 200–202. https://doi.org/10.1038/nature06912

Friedson, A. J. (1999). New observations and modelling of a QBO-like oscillation in Jupiter's stratosphere. *Icarus*, *137*, 34–55. https://doi.org/10.1006/icar.1998.6038

Friedson, A. J., & Moses, J. I. (2012). General circulation and transport in Saturn's upper troposphere and stratosphere. *Icarus*, *218*, 861–875. https://doi.org/10.1016/j.icarus.2012.02.004

Garcia, R. R., Dunkerton, T. J., Lieberman, R. S., & Vincent, R. A. (1997). Climatology of the semiannual oscillation of the tropical middle atmosphere. *Journal of Geophysical Research*, *102*, 26,019–26,032. https://doi.org/10.1029/97JD00207

García-Melendo, E., Sánchez-Lavega, A., Legarreta, J., Perez-Hoyos, S., & Hueso, R. (2010). A strong high altitude narrow jet detected at Saturn's equator. *Geophysical Research Letters*, *37*, L22204. https://doi.org/10.1029/2010GL045434

Guerlet, S., Fouchet, T., Bézard, B., Flasar, F. M., & Simon-Miller, A. A. (2011). Evolution of the equatorial oscillation in Saturn's stratosphere between 2005 and 2010 from Cassini/CIRS limb data analysis. *Geophysical Research Letters*, *38*, L09201. https://doi.org/10.1029/2011GL047192

Guerlet, S., Fouchet, T., Bézard, B., Simon-Miller, A. A., & Michael Flasar, F. (2009). Vertical and meridional distribution of ethane, acetylene and propane in Saturn's stratosphere from CIRS/Cassini limb observations. *Icarus*, *203*, 214–232. https://doi.org/10.1016/j.icarus.2009.04.002

Guerlet, S., Spiga, A., Sylvestre, M., Indurain, M., Fouchet, T., Leconte, J., … Forget, F. (2014). Global climate modeling of Saturn's atmosphere. Part I: Evaluation of the radiative transfer model. *Icarus*, *203*, 214–232. https://doi.org/10.1016/j.icarus.2014.05.010

Holton, J. R., & Lindzen, R. S. (1972). An updated theory for the quasi-biennial cycle of the tropical stratosphere. *Journal of Atmospheric Sciences*, *29*, 1076–1080. https://doi.org/10.1175/1520-0469(1972)029<1076:AUTFTQ>2.0.CO;2

Leovy, C. B., Friedson, A. J., & Orton, G. S. (1991). The quasiquadrennial oscillation of Jupiter's equatorial stratosphere. *Nature*, *354*, 380–382. https://doi.org/10.1038/354380a0

Li, X., & Read, P. L. (2000). A mechanistic model of the quasi-quadrennial oscillation in Jupiter's stratosphere. *Planetary and Space Sciences*, *48*, 637–669. https://doi.org/10.1016/S0032-0633(00)00033-7

Liming, L., Gierasch, P. J., Achterberg, R. K., Conrath, B. J., Flasar, F. M., Vasavada, A. R., … Fletcher, L. N. (2008). Strong jet and a new thermal wave in Saturn's equatorial stratosphere. *Geophysical Research Letters*, *35*, L23208. https://doi.org/10.1029/2008GL035515

Matsuno, T. (1966). Quasi-geostrophic motions in the equatorial area. *Journal of the Meteorological Society of Japan*, *44*, 25–43.

Moses, J. I., Bézard, B., Lellouch, E., Gladstone, G. R., Feuchtgruber, H., & Allen, M. (2000). Photochemistry of Saturn's atmosphere. I. Hydrocarbon chemistry and comparisons with ISO observations. *Icarus*, *143*, 244–298. https://doi.org/10.1006/icar.1999.6270

Ortiz, J. L., Orton, G. S., Friedson, A. J., Stewart, S. T., Fisher, B. M., & Spencer, J. R. (1998). Evolution and persistence of 5-μm hot spots at the Galileo probe entry latitude. *Journal of Geophysical Research*, *103*, 23,051–23,069. https://doi.org/10.1029/98JE00696

Orton, G. S., & Yanamandra-Fisher, P. A. (2005). Saturn's temperature field from high-resolution middle-infrared imaging. *Science*, *307*, 696–698. https://doi.org/10.1126/science.1105730

Orton, G. S., Fletcher, L. N., Flasar, F., Achterberg, R. K., Yanamandra-Fisher, P. A., Lewis, M., … Brown, S. K. (2013). Properties of slowly moving thermal waves in saturn from Cassini CIRS and ground-based thermal observations from 2003 to 2009. In *AAS/Division for Planetary Sciences Meeting Abstracts, AAS/Division for Planetary Sciences Meeting Abstracts* (Vol. 45, p. 312.07).

Orton, G. S., Yanamandra-Fisher, P. A., Fisher, B. M., Friedson, A. J., Parrish, P. D., Nelson, J. F., … Tollestrup, E. (2008). Semi-annual oscillations in Saturn's low-latitude stratospheric temperatures. *Nature*, *453*, 196–199. https://doi.org/10.1038/nature06897

Sánchez-Lavega, A., García-Melendo, E., Pérez-Hoyos, S., Hueso, R., Wong, M. H., Simon, A., … Barry, T. (2016). An enduring rapidly moving storm as a guide to Saturn's equatorial jet's complex structure. *Nature Communications*, *7*, 13262. https://doi.org/10.1038/ncomms13262

Schinder, P. J., Flasar, F. M., Marouf, E. A., French, R. G., McGhee, C. A., Kliore, A. J., … Anabtawi, A. (2011). Saturn's equatorial oscillation: Evidence of descending thermal structure from Cassini radio occultations. *Geophysical Research Letters*, *38*, L08205. https://doi.org/10.1029/2011GL047191

Sinclair, J. A., Irwin, P. G. J., Fletcher, L. N., Greathouse, T., Guerlet, S., Hurley, J., & Merlet, C. (2014). From Voyager-IRIS to Cassini-CIRS: Interannual variability in Saturn's stratosphere? *Icarus*, *233*, 281–292. https://doi.org/10.1016/j.icarus.2014.02.009

Spiga, A., Guerlet, S., Meurdesoif, Y., Indurain, M., Millour, E., Sylvestre, M., … Fouchet, T. (2016). Jets, eddies and waves in Saturn's troposphere and stratosphere from multi-annual high-resolution Global Climate Modeling. In *AAS/Division for Planetary Sciences Meeting Abstracts, AAS/Division for Planetary Sciences Meeting Abstracts* (Vol. 48, p. 421.20).

Sylvestre, M., Guerlet, S., Fouchet, T., Spiga, A., Flasar, F. M., Hesman, B., & Bjoraker, G. L. (2015). Seasonal changes in Saturn's stratosphere inferred from Cassini/CIRS limb observations. *Icarus*, *258*, 224–238. https://doi.org/10.1016/j.icarus.2015.05.025

Takahashi, M., & Holton, J. R. (1991). The mean zonal flow response to rossby wave and gravity wave forcing in the equatorial lower stratosphere: Relationship to the QBO. *Journal of Atmospheric Sciences*, *48*, 2078–2088.

Yang, G.-Y., Hoskins, B., & Gray, L. (2012). The influence of the QBO on the propagation of equatorial waves into the stratosphere. *Journal of Atmospheric Sciences*, *69*, 2959–2982. https://doi.org/10.1175/JAS-D-11-0342.1